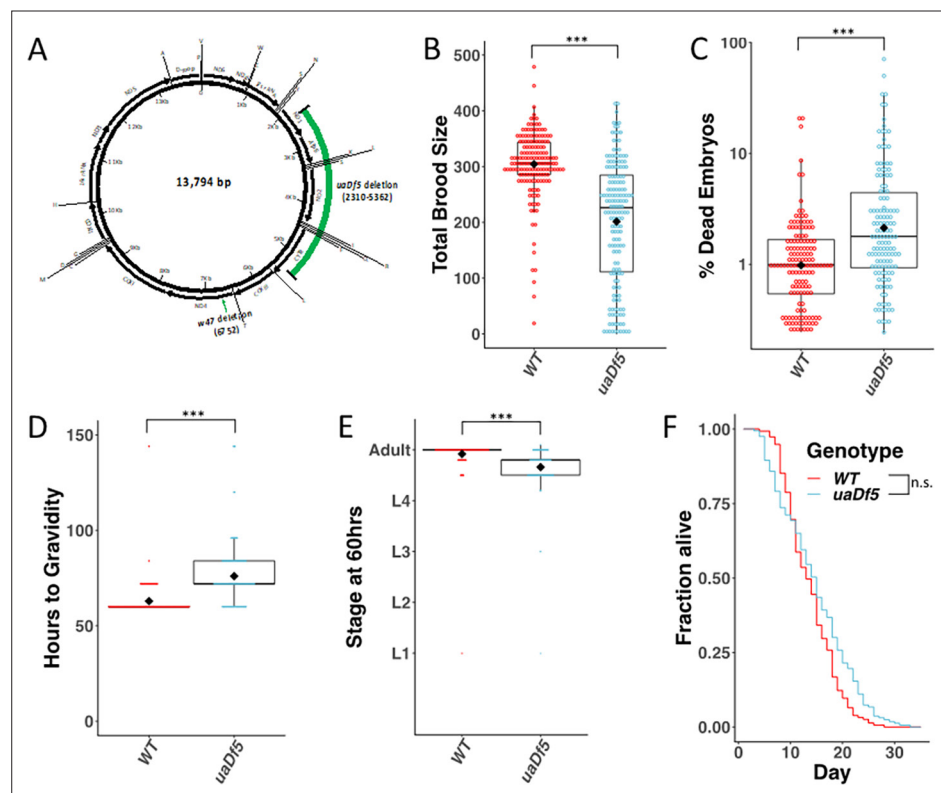


---

## Figures and figure supplements

Regulation of defective mitochondrial DNA accumulation and transmission in *C. elegans* by the programmed cell death and aging pathways

**Sagen Flowers et al.**



**Figure 1.** Analysis of the impact of mtDNA<sup>uaDf5</sup> on fitness parameters. **(A)** Diagram of *C. elegans* mtDNA. Black bars with arrows indicate the locations of genes and direction of transcription. Black lines with letters indicate the locations of tRNAs. Green bars show the locations of the mtDNA<sup>uaDf5</sup> deletion as well as the linked w47 insertion that was identified via Illumina sequencing. **(B)** Brood size analysis of mtDNA<sup>uaDf5</sup> compared to laboratory wildtype N2. **(C)** Embryonic lethality analysis of mtDNA<sup>uaDf5</sup> compared to laboratory wildtype N2. **(D)** Developmental rate analysis of mtDNA<sup>uaDf5</sup> compared to laboratory wildtype N2, counting how many hours it takes for starved L1s to reach gravidity once plated on food. **(E)** Developmental rate analysis of mtDNA<sup>uaDf5</sup> compared to laboratory wildtype N2, staging worms 60 hr after synchronized, starved L1s are plated on food. **(F)** Survival curve analysis of mtDNA<sup>uaDf5</sup> compared to laboratory wildtype N2, day 1 is defined as the day starved L1s are plated on food. Median lifespan and statistics are presented in **Figure 1—figure supplement 2**. For **(B–E)**, box plots show median and IQR (Interquartile Range), and the diamond indicates the mean. Statistical analysis was performed using the Mann–Whitney test (\*\*\*)  $p < 0.001$ , n.s. not significant).

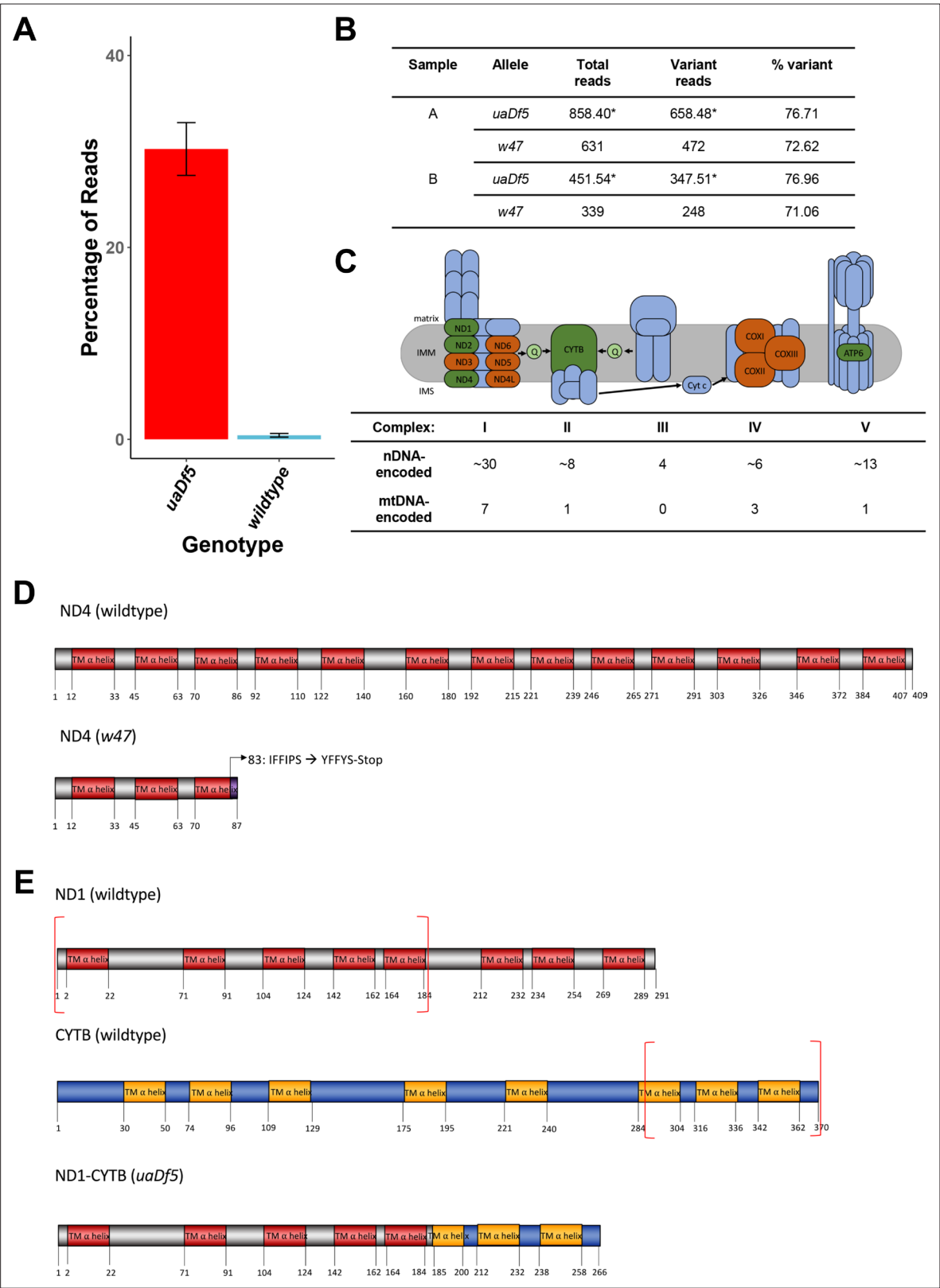
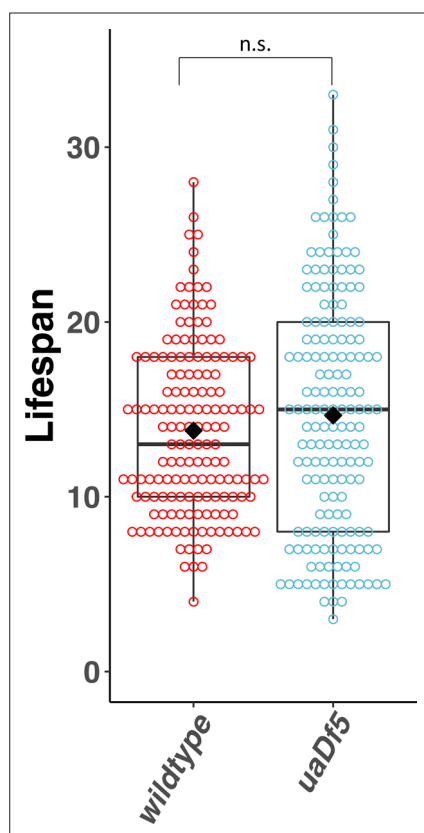


**Figure 1—figure supplement 1.** Characterization of the *uaDf5* allele. **(A)** The percentage of reads that mapped to the *w47* insertion in *uaDf5* samples (red) and wildtype samples (blue). Error bars represent standard deviation of the mean (SEM). **(B)** Table outlining the percentage of reads that mapped to the *w47* and *uaDf5* mutations in *uaDf5* samples. \*The number of variant reads was determined by averaging the mapped reads across the deleted region and subtracting that from the average number of reads mapped to the rest of the mtDNA genome (total reads). **(C)** Diagram showing

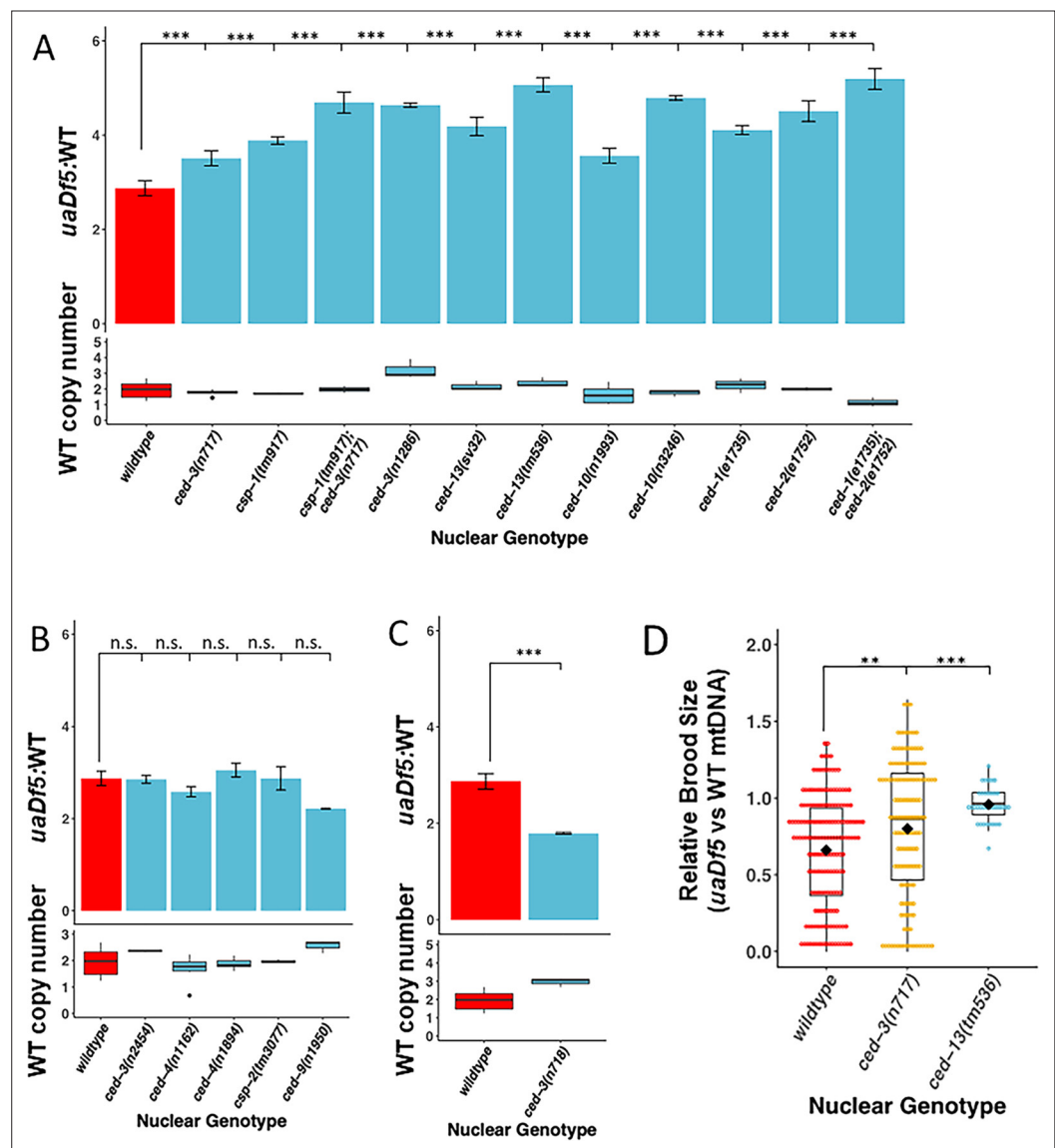
Figure 1—figure supplement 1 continued on next page

*Figure 1—figure supplement 1 continued*

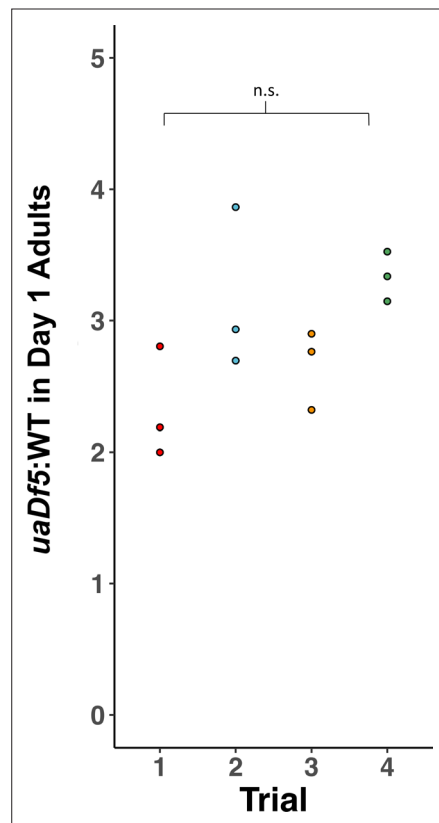
the mitochondrial respiratory chain (MRC) machinery subunits. Blue indicates nuclear DNA (nDNA)-encoded subunits, orange and green indicate mtDNA-encoded subunits. Green indicates those subunits that are knocked out in the *uaDf5* allele (including NADH dehydrogenase 4 [ND4] which is knocked out by the linked *w47* mutation). **(D)** Diagram showing the likely effect of the *w47* mutation on ND4 protein translation. ND4 is a 409-aa long transmembrane subunit that spans the inner mitochondrial membrane 13 times. The *w47* mutation results in a premature stop codon at position 89, eliminating 10 of the 13 alpha-helix membrane domains. **(E)** Diagram showing the likely effect of the *uaDf5* mutation on ND1 protein translation. ND1 is a 291-aa long transmembrane subunit that spans the inner mitochondrial membrane 8 times and CYTB is a 370-aa long transmembrane subunit that spans the inner mitochondrial membrane 8 times. The *uaDf5* mutation results in a 266 amino acid long fusion protein that connects the first 185 amino acids (and 5 subunits) of ND1 with the last 81 amino acids (and 3 subunits) of CYTB.



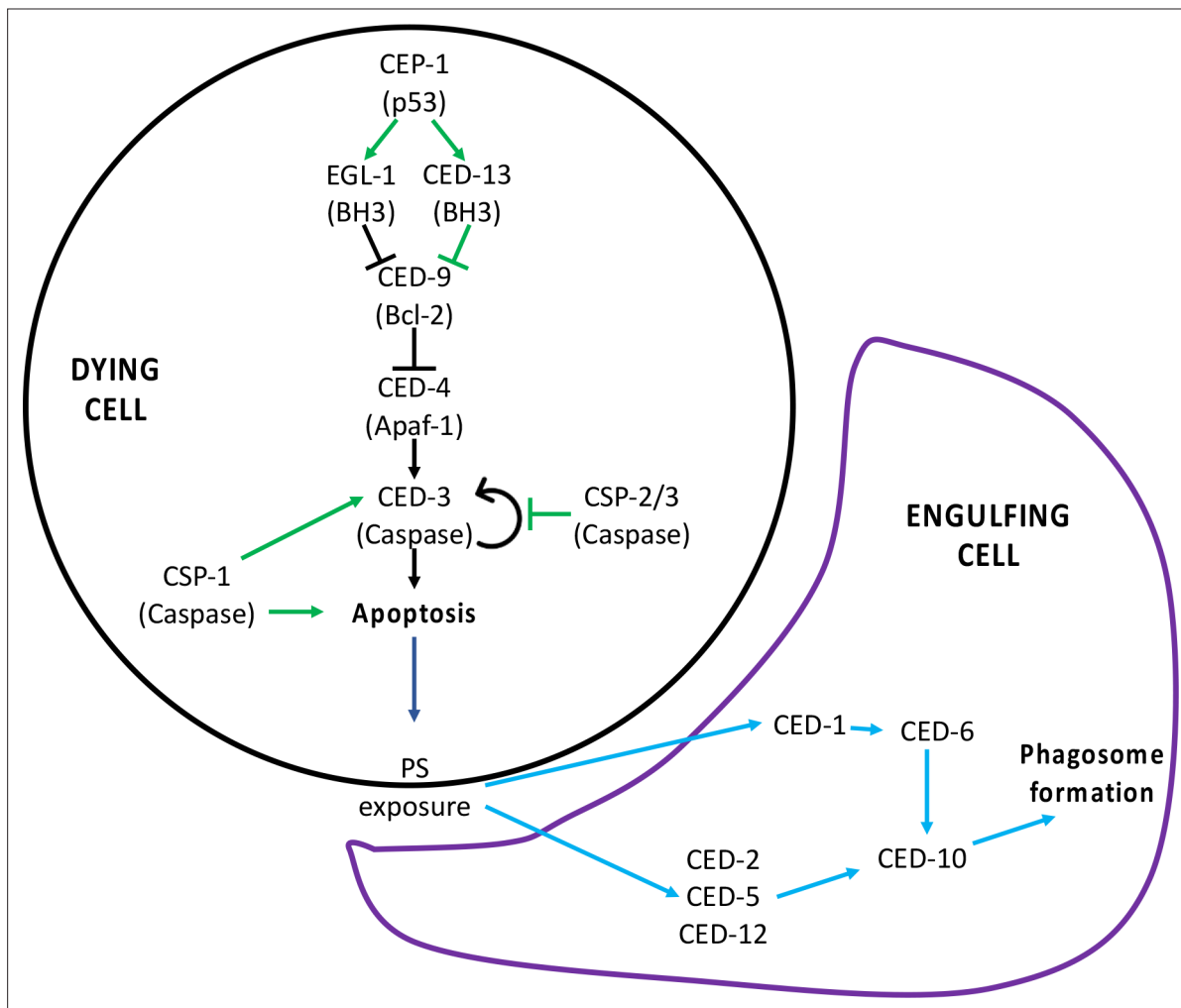
**Figure 1—figure supplement 2.** Lifespan analysis of the impact of *uaDf5*. Lifespan analysis of N2-bearing *uaDf5* compared to wildtype N2. Day 1 is defined as the day starved L1s are plated on food. Box plots show median and IQR, and the diamond indicates the mean. Statistical analysis was performed using the Mann–Whitney test (n.s., not significant).



**Figure 2.** Regulators of programmed cell death (PCD) act on mutant mtDNA. (A–C) Digital-droplet PCR (ddPCR) analysis of the steady-state molar ratio of mtDNA<sup>*uaDf5*</sup> in 200 worm populations of day 1 adults of various PCD mutant backgrounds. (A) PCD mutants that result in a significant increase in the molar ratio of mtDNA<sup>*uaDf5*</sup>. (B) PCD mutants that result in no statistical change in the molar ratio of mtDNA<sup>*uaDf5*</sup>. (C) PCD mutant that results in a significant decrease in the molar ratio of mtDNA<sup>*uaDf5*</sup>. (D) The relative brood size of the animals with and without mtDNA<sup>*uaDf5*</sup> in the indicated mutant backgrounds. For each nuclear genotype shown, the brood size of *uaDf5*-containing worms was normalized by dividing by the average brood size of worms containing only WT-mtDNA. Box plots show the median and IQR, the diamond indicates the mean. For A–C, *n* = 3 or more biological replicates of 200 worm populations were performed for each genotype. Average wildtype mtDNA copy number ± standard deviation is shown in the graph below in each panel. Statistical analysis was performed using one-way analysis of variance (ANOVA) with Dunnett's correction for multiple comparisons. For (D), statistical analysis was performed using the Mann–Whitney test. Error bars represent standard deviation of the mean (SEM) (\*\*\**p* < 0.001, \*\**p* < 0.01, \**p* < 0.05, n.s. not significant).



**Figure 2—figure supplement 1.** Reproducibility of digital-droplet PCR (ddPCR) measurement of *uaDf5*. Analysis of the steady state of *uaDf5* in a wildtype nuclear background shows highly stable steady-state levels. Trials were done months apart on different thaws. Dots represent biological replicates. Statistical analysis was performed using one-way analysis of variance (ANOVA) with Tukey correction for multiple comparisons (n.s., not significant).

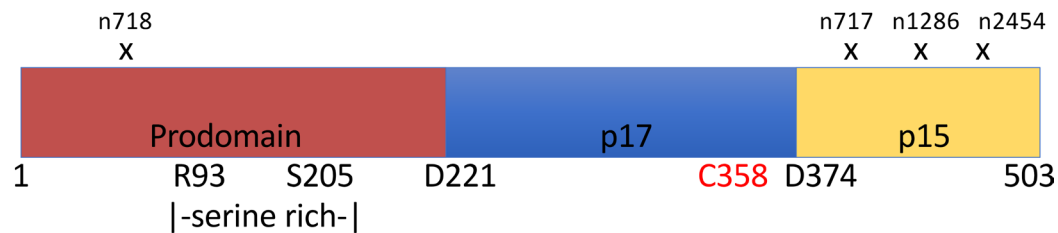


**Figure 2—figure supplement 2.** Programmed cell death (PCD) signaling pathway. **(A)** Signaling pathway for PCD. The canonical pathway is shown with black arrows, the non-canonical pathway is shown with green arrows, and the downstream engulfment pathway is shown with blue arrows. Figure supplement 2 has been adapted from Figure 2 in *Conradt et al., 2016*.



**A**

Allele	Location	Domain	Level of <i>uaDf5</i>
<i>n1286</i>	W428opal	p15	highest
<i>n717</i>	Position 403 - Exon 7 acceptor	p15	high
<i>n2454</i>	A466T	p15	unchanged
<i>n718</i>	G65R	Prodomain	low

**B**

**Figure 2—figure supplement 3.** Analysis of the *ced-3* alleles. (A) Locations and consequences of the four tested *ced-3* alleles, as well as the measured fractional abundance of *uaDf5*. (B) Diagram showing the locations of the mutations for each allele.

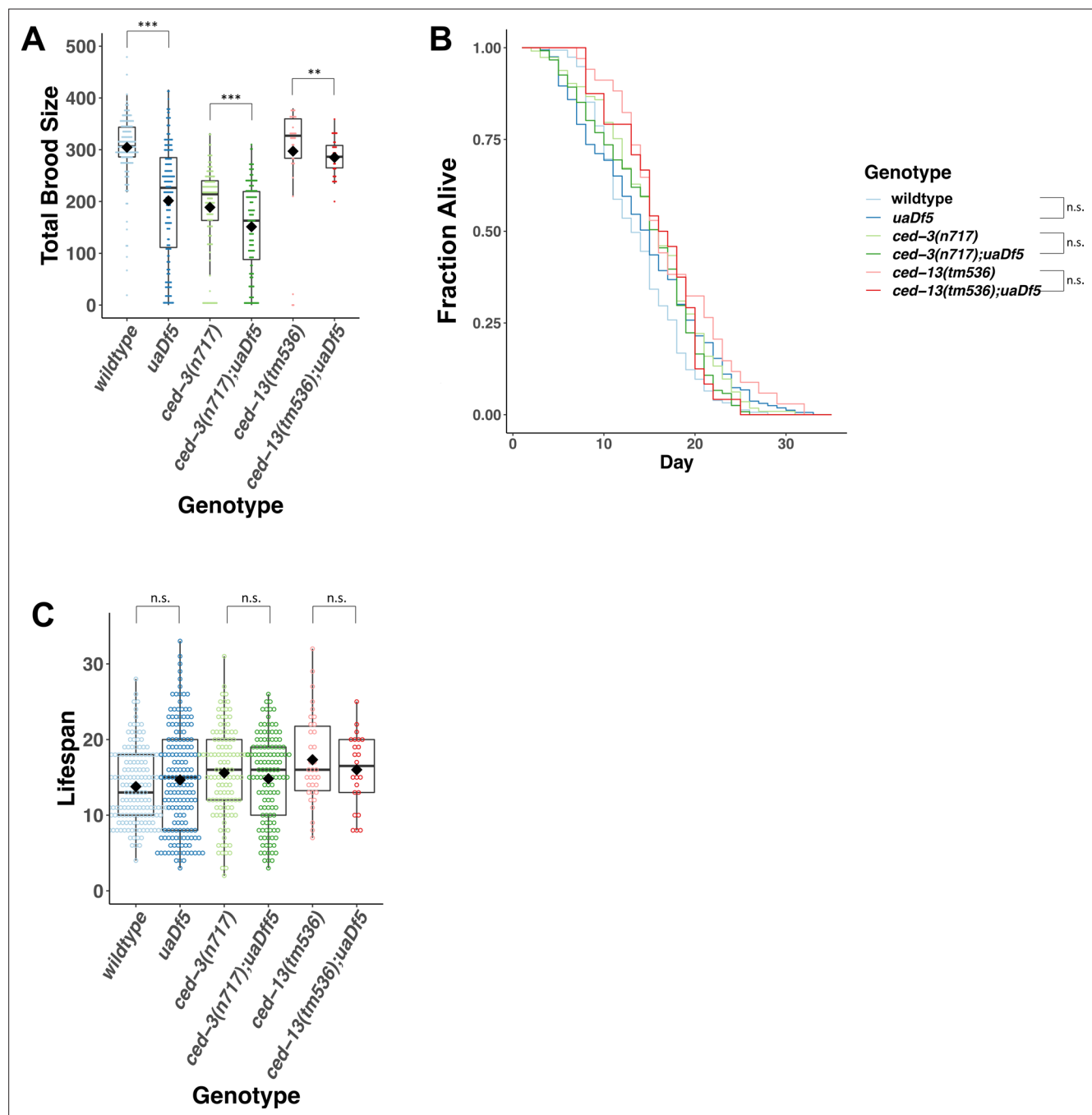


**Figure 2—figure supplement 4.** Analysis of the impact of *uaDf5* on fitness parameters in programmed cell death (PCD) mutants. **(A)** Brood size analysis of PCD mutants. **(B)** Lifespan analysis shows that *uaDf5* does not affect lifespan in both wildtype background and in PCD mutant backgrounds. **(C)** Lifespan analysis shows that *uaDf5* does not affect lifespan in a wildtype nuclear background nor in PCD mutant backgrounds. For **B** and **C**, day 1 is defined as the day starved L1s are plated on food. For **A** and **C**, box plots show median and IQR, and the diamond indicates the mean. Statistical analysis was performed using the Mann–Whitney Wilcoxon test (\*\* $p < 0.001$ , \*\* $p < 0.01$ , n.s., not significant).

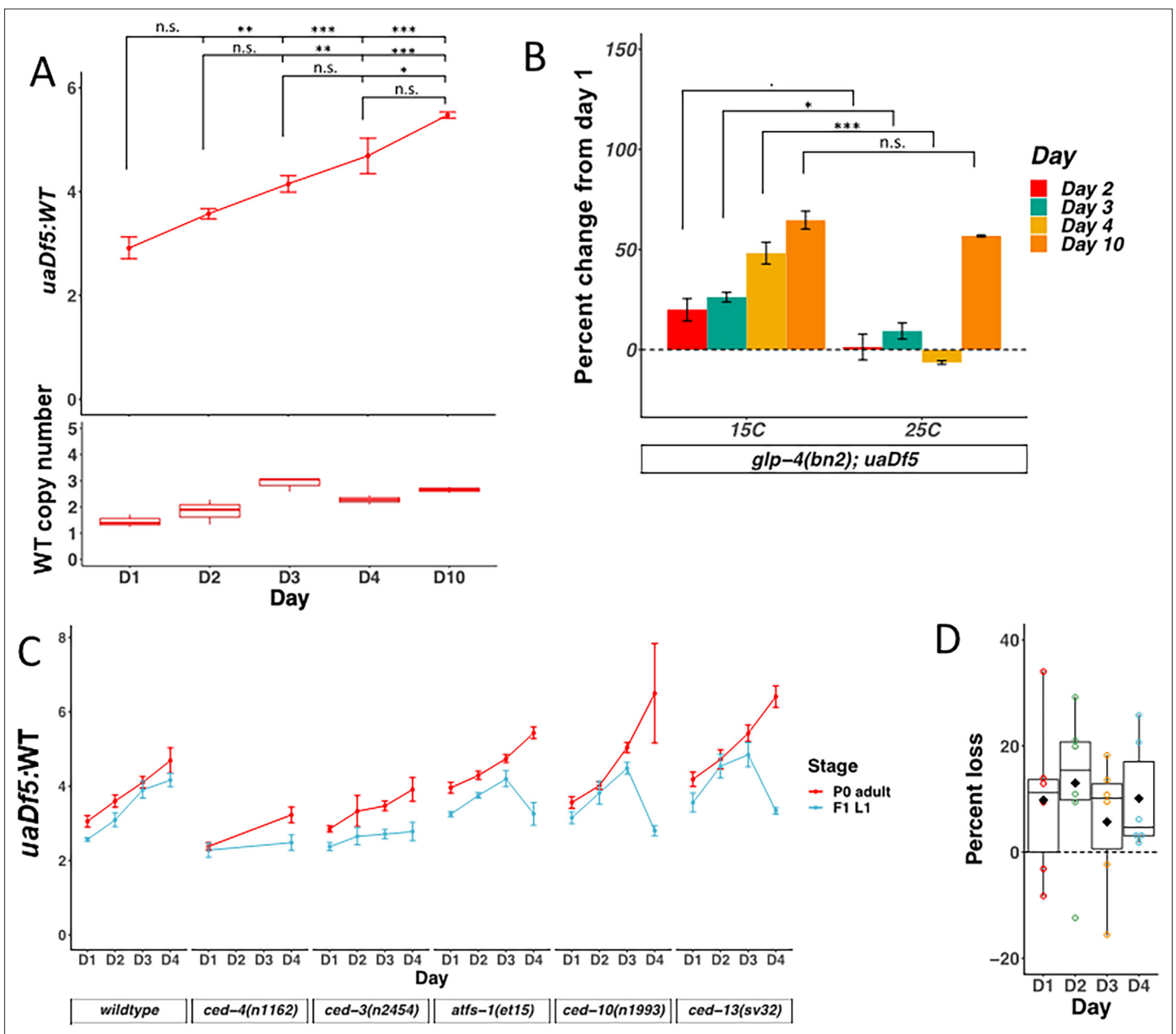


**Figure 3.** mtDNA<sup>uaDf5</sup> accumulates in the germline of aging adults, and evidence of purifying selection between mother and offspring. **(A)** Analysis of the molar ratio of mtDNA<sup>uaDf5</sup> in aging adults in a wildtype nuclear background. Average wildtype mtDNA copy number  $\pm$  standard deviation is shown in the graph below. **(B)** Analysis of the percent change of *uaDf5*:WT from day 1 (Y axis = (*uaDf5*:WT day x - *uaDf5*:WT day 1)/(*uaDf5*:WT day 1)). For *glp-1(q231ts)*, *fem-3(q20ts)*, and *glp-4(bn2ts)*, 15°C is the permissive temperature (germline development occurs) and 25°C is the restrictive temperature (female germline development is inhibited). Statistical analysis was performed using one-way analysis of variance (ANOVA) with Tukey correction for multiple comparisons (\*\*\*p < 0.001, \*\*p < 0.01, \*p < 0.05, n.s., not significant). Error bars represent standard deviation of the mean (SEM). **(C)** Analysis of the molar ratio of mtDNA<sup>uaDf5</sup> in aging adults (P0 adult) and their L1 progeny (F1-L1) in various nuclear backgrounds shows that all strains decrease the *uaDf5* load during transmission from mother to offspring, and that strains with significantly higher mtDNA<sup>uaDf5</sup> levels (*atfs-1(et15)*, *ced-10(n1993)*, and *ced-13(sv32)*) have a more significant removal mechanism at day 4 of adulthood. n = 3 or more replicates of 200 worm populations were performed for each timepoint. Error bars represent SEM. Gray dashed line indicates a hypothetical threshold at which high mtDNA<sup>uaDf5</sup> burden activates enhanced intergenerational purifying selection in older mothers. **(D)** Analysis of the measured loss of mtDNA<sup>uaDf5</sup> between mother and offspring at each day of adulthood shows that mtDNA<sup>uaDf5</sup> removal occurs. n = 6 replicates of 200 worm populations for each condition.

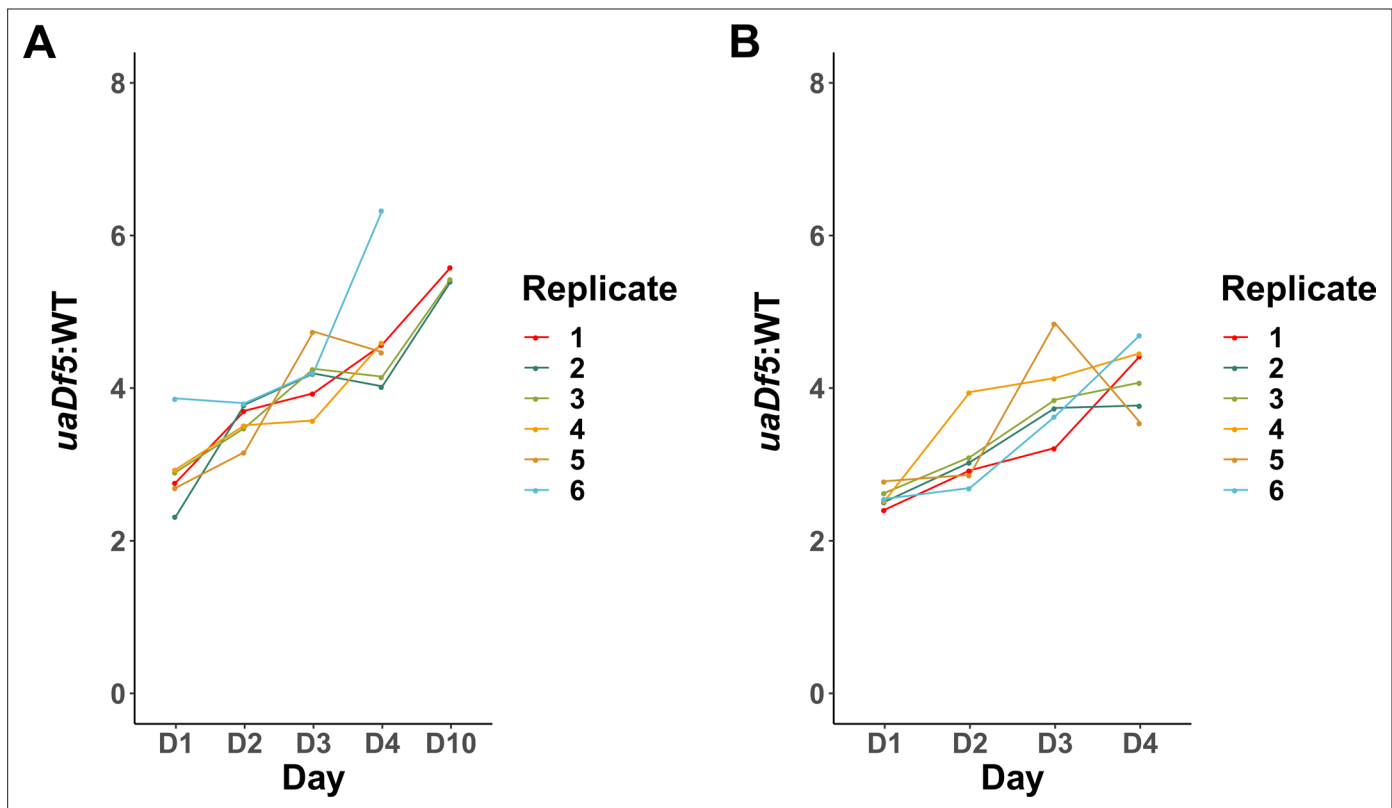


**Figure 3—figure supplement 1.** *uaDf5* accumulation in individual lines of adults and progeny. **(A)** Analysis of *uaDf5* accumulation in individual lines of aging P0 adults shows a consistent accumulation trend as adults age. **(B)** Analysis of *uaDf5* accumulation in individual lines of F1-L1 progeny that were born from those mothers shown in panel A shows a consistent trend of progeny born from older mothers inheriting a larger *uaDf5* load than their siblings born from younger mothers.

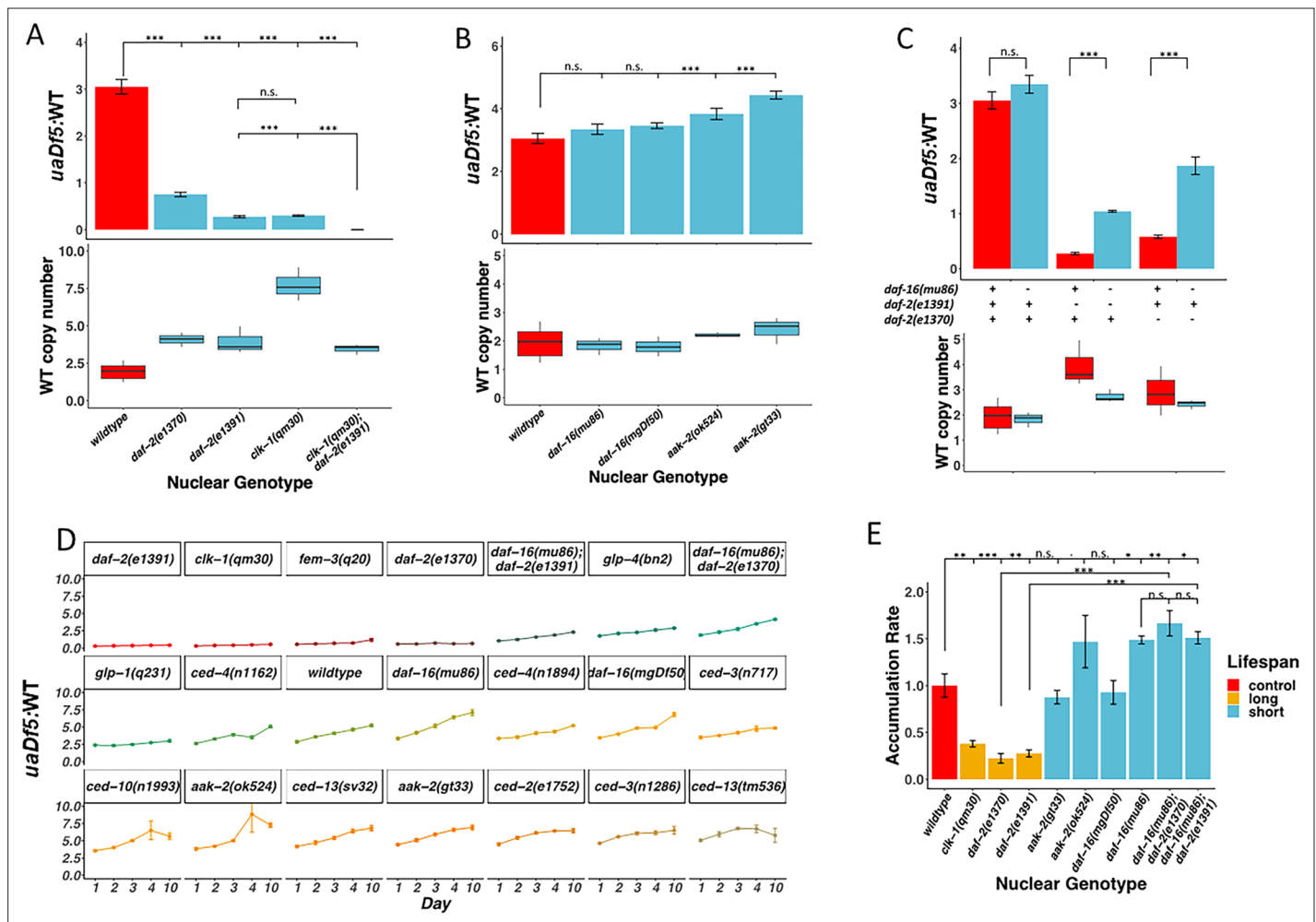


**Figure 4.** Lifespan mutants have both a lower steady-state level and accumulation rate of mtDNA<sup>uaDf5</sup>. (A–C) Analysis of molar ratio of mtDNA<sup>uaDf5</sup> in day 1 adults of various mutant backgrounds. Average wildtype mtDNA copy number  $\pm$  standard deviation is shown in the graph below in each panel. (A) Analysis of steady-state mtDNA<sup>uaDf5</sup> levels in long-lived mutants. (B) Analysis of steady-state mtDNA<sup>uaDf5</sup> levels in short-lived mutants, showing synergistic activity on mtDNA<sup>uaDf5</sup> removal capacity in the *daf-2(e1391) clk-1(qm30)* double mutant. (C) Analysis of steady-state mtDNA<sup>uaDf5</sup> levels in *daf-2(-)* single and *daf-16(-)*; *daf-2(-)* double mutants, showing a partial rescue of *daf-2(-)* phenotype by *daf-16(-)*. (D) Analysis of the molar ratio of mtDNA<sup>uaDf5</sup> in aging adults in 21 different nuclear backgrounds shows a consistent accumulation trend. (E) Summary of the rate of increase for the lifespan regulation mutants, showing that *daf-16* rescues the *daf-2* accumulation rate phenotype. The normalized accumulation rate was calculated by fitting a regression line for each trial and then dividing the slope of the regression line by the slope of the averaged regression line found in a wildtype background. For all,  $n = 3$  or more replicates of 200 worm populations for each genotype and stage. For **A** and **E**, statistical analysis was performed using one-way analysis of variance (ANOVA) with Tukey correction for multiple comparisons. For **C**, statistical analysis was performed using one-way ANOVA. For **B**, statistical analysis was performed using one-way ANOVA with Dunnett's correction for multiple comparisons. Error bars represent standard deviation of the mean (SEM) (\*\* $p < 0.001$ , \* $p < 0.01$ ,  $p < 0.05$ , n.s., not significant).

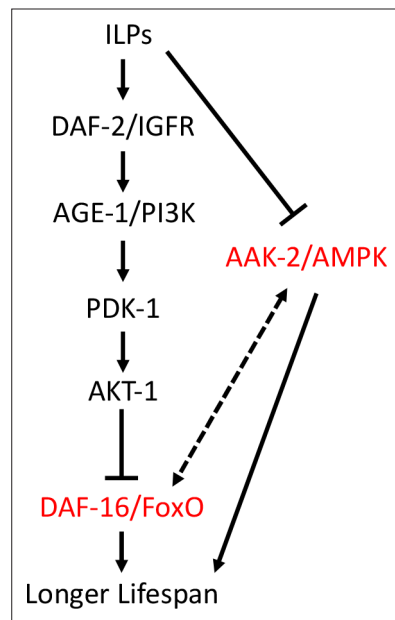


**Figure 4—figure supplement 1.** Insulin/IGF-1 signaling (IIS) pathway. Insulin-like peptides (ILPs) bind to DAF-2 and activate the PI3P pathway which prevents nuclear translocation of DAF-16. AAK-2 may phosphorylate and activate DAF-16 transcriptional activity. Loss of *aak-2* or *daf-2* (highlighted in red) reduces lifespan.

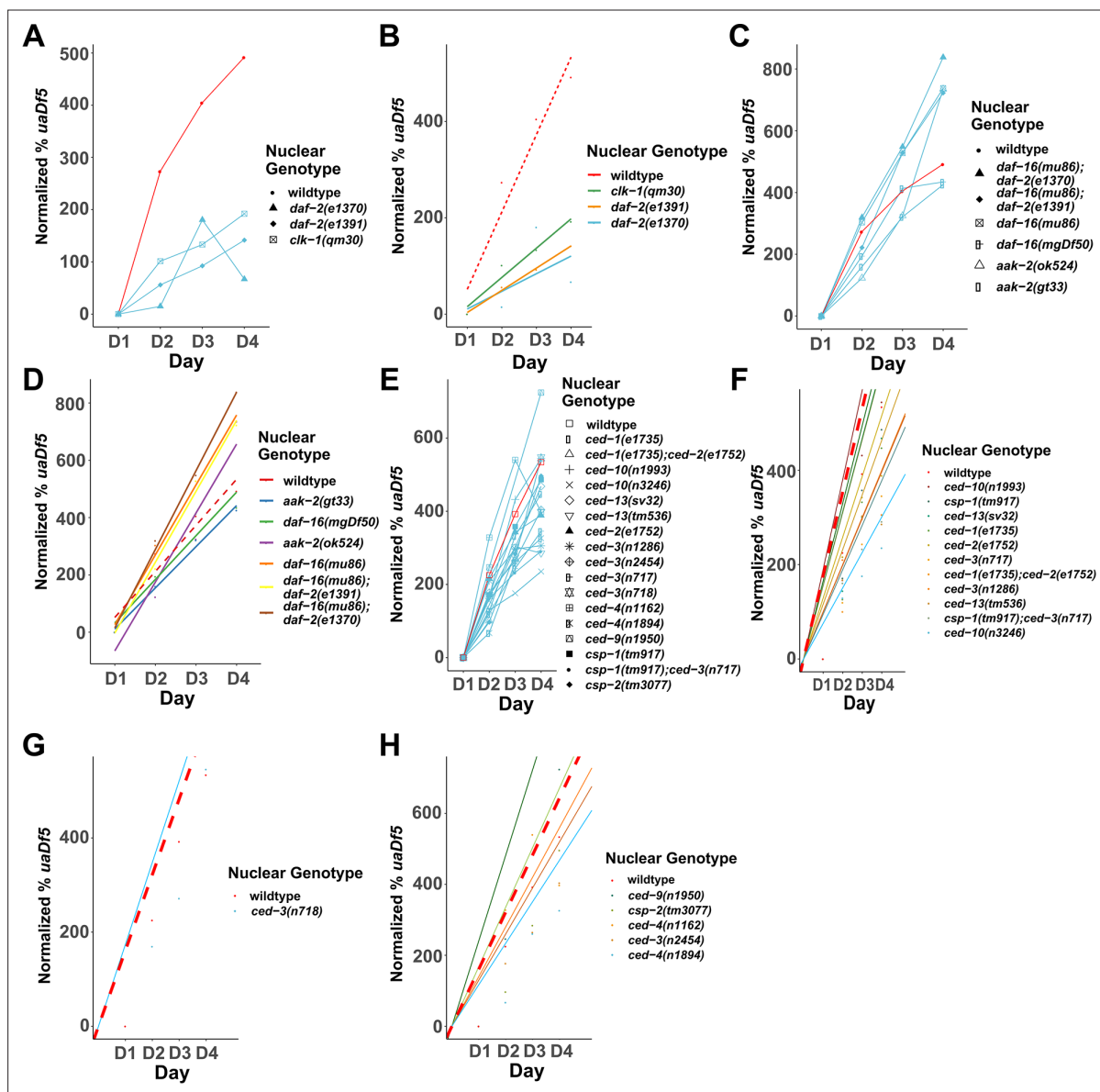


**Figure 4—figure supplement 2.** Analysis of the accumulation of mtDNA<sup>uaDf5</sup> in programmed cell death (PCD) and lifespan mutants. Analysis of the normalized fractional abundance *uaDf5* [(% *uaDf5* day *x* – % *uaDf5* day 1) × % *uaDf5* day 1] in steady-state populations, showing the accumulation rate of mtDNA<sup>uaDf5</sup> as worms age from day 1 to 4 of adulthood. (A, B) Analysis of the accumulation of *uaDf5* in long-lived mutants. (C) Analysis of the accumulation of mtDNA<sup>uaDf5</sup> in short-lived mutants (C, D). Linear regression analysis of the normalized fractional abundance *uaDf5* [(% *uaDf5* day *x* – % *uaDf5* day 1) × % *uaDf5* day 1] in steady-state populations, showing the accumulation rate of mtDNA<sup>uaDf5</sup> as worms age from day 1 to 4 of adulthood. (C) Analysis of long-lived mutants. (D) Analysis of short-lived mutants. (E) Analysis of the accumulation of mtDNA<sup>uaDf5</sup> in PCD mutants. (F–H) Linear regression analysis of the normalized fractional abundance mtDNA<sup>uaDf5</sup> [(% *uaDf5* day *x* – % *uaDf5* day 1) × % *uaDf5* day 1] in steady-state populations, showing the accumulation rate of mtDNA<sup>uaDf5</sup> as worms age from day 1 to 4 of adulthood. (F) Analysis of PCD mutants with significantly high steady-state level of mtDNA<sup>uaDf5</sup>. (G) Analysis of PCD mutants with significantly low steady-state level of mtDNA<sup>uaDf5</sup>. (H) Analysis of PCD mutants with no significant change in the steady-state level of mtDNA<sup>uaDf5</sup>. For C, D, F–H, dots represent actual datapoints, lines are fitted regression models of the data. For all, *n* = 3 replicates or more of 200 worm populations for each datapoint.

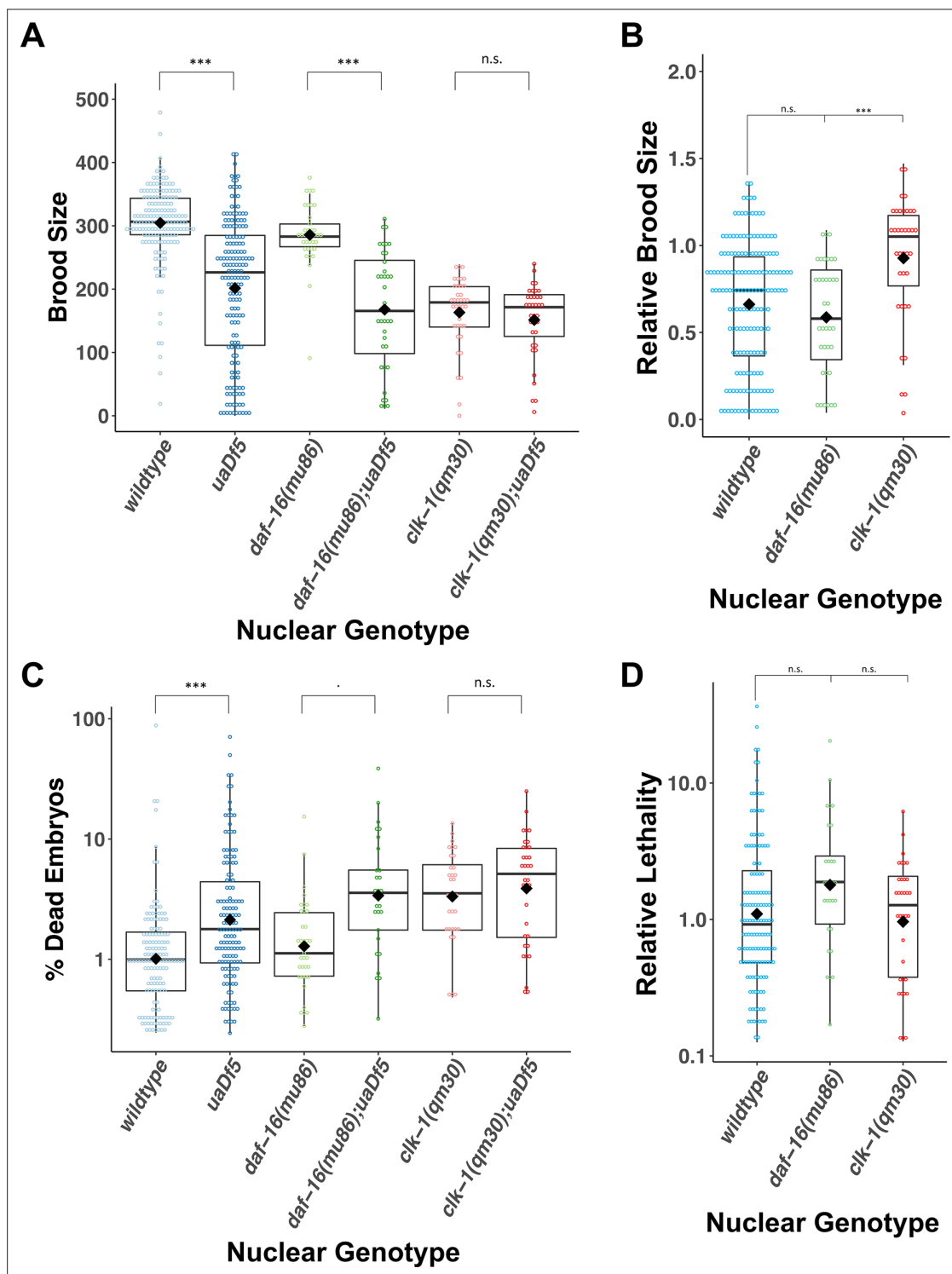


**Figure 4—figure supplement 3.** *uaDf5* differentially impacts fitness parameters in lifespan-affecting mutants. (**A**, **B**) Brood size analysis showing how *uaDf5* differentially impacts brood size in lifespan mutant backgrounds. *uaDf5* has no negative impact on the long-lived mutant *clk-1* but has a modestly larger negative impact on the short-lived mutant *daf-16* than it does in the wildtype background. (**B**) Relative brood size of the animals with and without *uaDf5* in the indicated mutant backgrounds. (**C**, **D**) Embryonic lethality analysis showing how *uaDf5* differentially impacts embryonic lethality in lifespan mutant backgrounds. *uaDf5* has no negative impact on the long-lived mutant *clk-1* but has a modestly larger negative impact on the short-lived mutant *daf-16* than it does in a wildtype background. (**D**) Relative lethality of the animals with and without *uaDf5* in the indicated mutant backgrounds. Box plots show median and IQR, and the diamond indicates the mean. For A and C, statistical analysis was performed using the Mann–Whitney test. For B and D, statistical analysis was performed using the Kruskal–Wallis test (\*\**p* < 0.001, n.s., not significant).



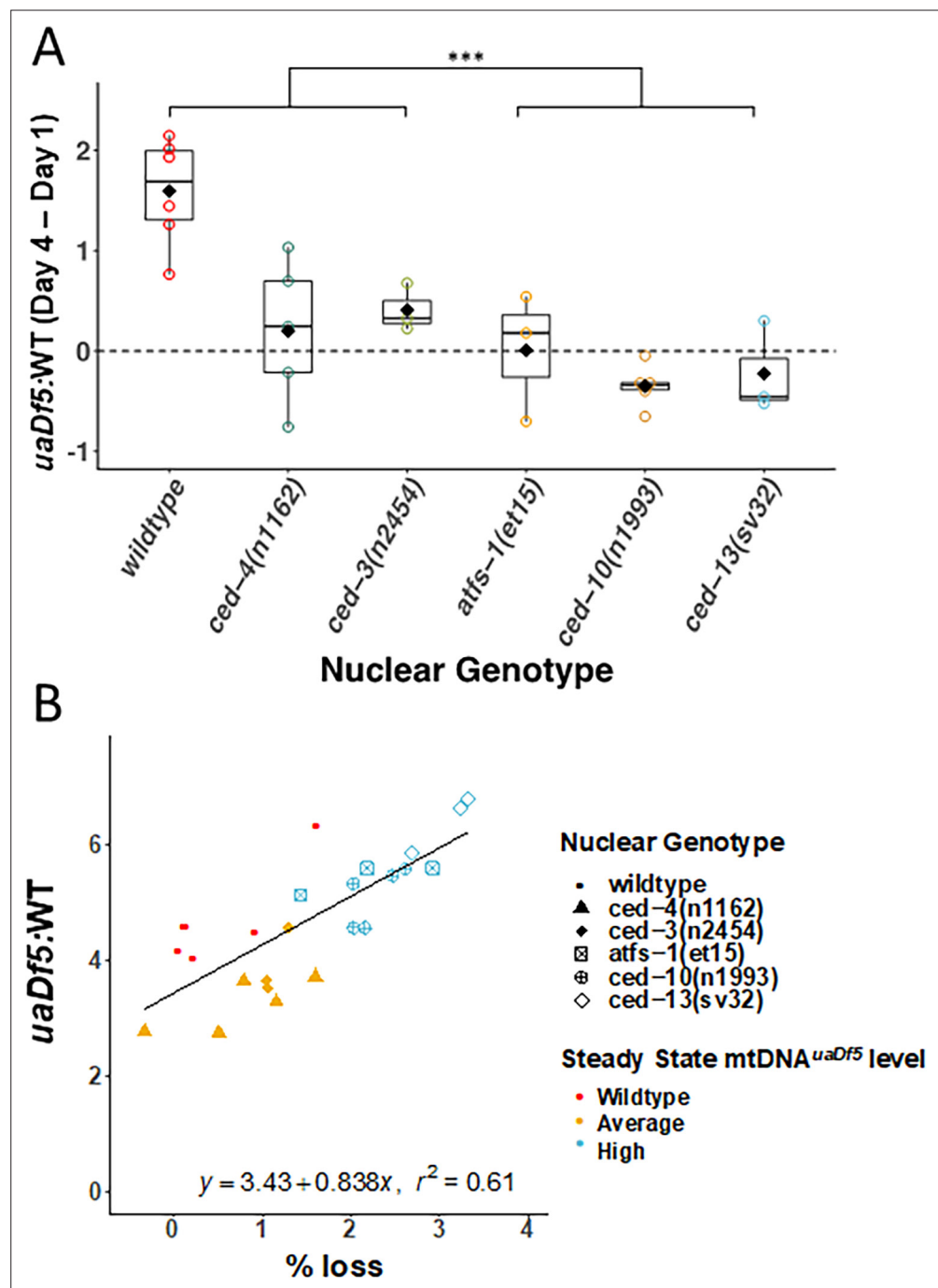


**Figure 5.** Evidence for late adulthood-specific mechanisms for removal of mtDNA<sup>uaDf5</sup>. **(A)** Subtracting *uaDf5*:WT in progeny from day 1 adults from progeny of day 4 adults shows that day 4 F1-L1s tend to have higher mtDNA<sup>uaDf5</sup> burden than their day 1 siblings, but this is no longer the case in nuclear backgrounds that result in a significantly higher steady-state levels of mtDNA<sup>uaDf5</sup> in the adult.  $n = 3$  or more replicates for each genotype and statistical analysis was performed using the Mann–Whitney test. **(B)** Comparison of the molar ratio of mtDNA<sup>uaDf5</sup> in day 4 adult mothers to the absolute % removal of mtDNA<sup>uaDf5</sup> from mother to offspring shows a positive correlation (\*\* $p < 0.001$ ).

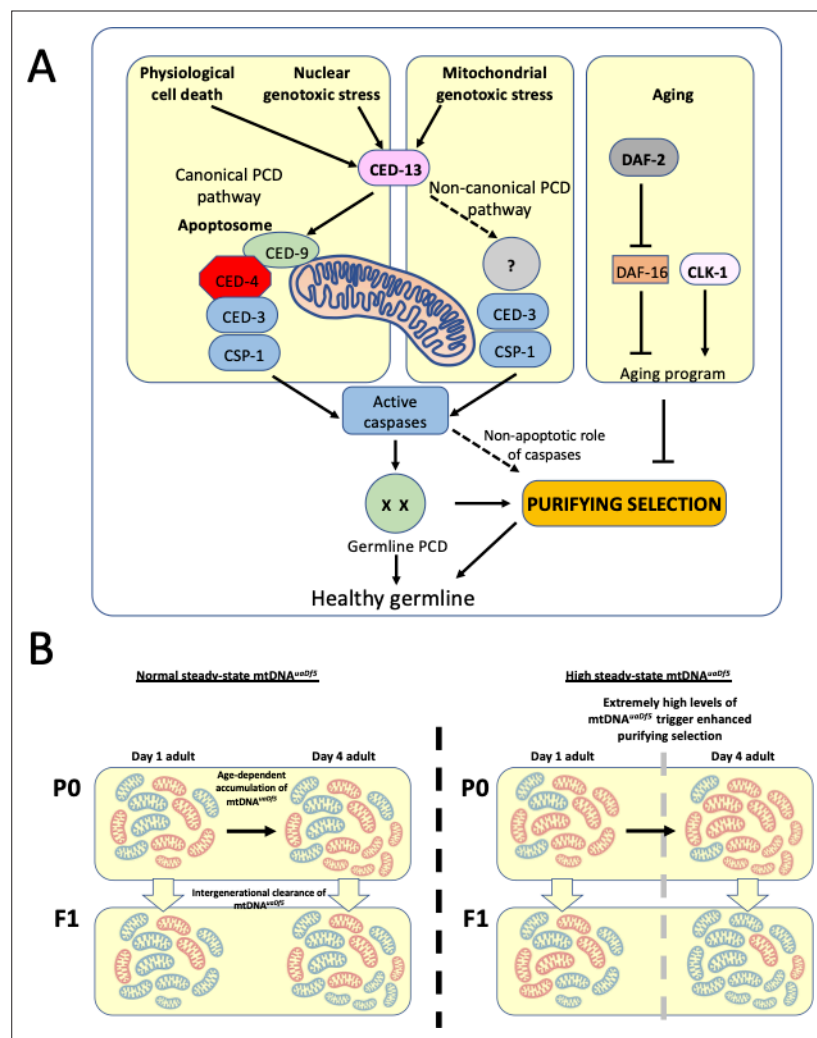


**Figure 6.** Regulation of mtDNA<sup>uaDf5</sup> accumulation and transmission by the programmed cell death (PCD) and aging pathways. **(A)** Our results suggest that CED-3 and CSP-1, which are activated by BH-3 only protein CED-13, function cooperatively to promote mitochondrial purifying selection, independent of CED-9 and the CED-4 apoptosome. The clearance of mtDNA<sup>uaDf5</sup> may therefore involve induction of a non-canonical germline PCD mechanism or non-apoptotic action of the CED-13/caspase axis. Additionally, Insulin/IGF-1 signaling (IIS) and CLK-1 aging pathways act synergistically to regulate mitochondrial purifying selection. **(B)** mtDNA<sup>uaDf5</sup> (red) accumulates in the germline relative to mtDNA<sup>WT</sup> (blue) as adults age and the increased mtDNA<sup>uaDf5</sup> levels are transmitted to the progeny, although the mtDNA<sup>uaDf5</sup> burden is consistently lower in progeny than mothers. This intergenerational purifying selection is enhanced in the older mothers of mutants with high steady-state mtDNA<sup>uaDf5</sup> (e.g., *ced-13*, *ced-10*, and *atfs-1*), suggesting a threshold beyond which a germline PCD-independent mtDNA quality control process may be initiated or enhanced in these older mothers.